LAWRENCE
LIVERMORE
NATIONAL
LABORATORY

LLNL-JRNL-447152

Kinetics of Ejected Particles During Laser-Induced Breakdown in Fused Silica

R. N. Raman, R. A. Negres, S. G. Demos

August 4, 2010

Applied Physics Letters

Disclaimer

This document was prepared as an account of work sponsored by an agency of the United States government. Neither the United States government nor Lawrence Livermore National Security, LLC, nor any of their employees makes any warranty, expressed or implied, or assumes any legal liability or responsibility for the accuracy, completeness, or usefulness of any information, apparatus, product, or process disclosed, or represents that its use would not infringe privately owned rights. Reference herein to any specific commercial product, process, or service by trade name, trademark, manufacturer, or otherwise does not necessarily constitute or imply its endorsement, recommendation, or favoring by the United States government or Lawrence Livermore National Security, LLC. The views and opinions of authors expressed herein do not necessarily state or reflect those of the United States government or Lawrence Livermore National Security, LLC, and shall not be used for advertising or product endorsement purposes.

Kinetics of ejected particles during laser-induced breakdown in fused silica

R. N. Raman, R. A. Negres, and S. G. Demos
Lawrence Livermore National Laboratory, 7000 East Ave., Livermore, California 94551

(Received

The kinetic properties of material clusters ejected during laser-induced breakdown on the surface of fused silica are temporally resolved. The experimental system involves the use of a time resolved microscope capable of acquiring two images at different time points of the material ejection process, allowing for a more accurate estimation of the particle size distribution, particle speed, changes in speed, and ejection time with respect to the incident laser pulse.

Laser-matter interactions are of fundamental importance in various applications such as laser ablation of materials, thin film laser deposition, and laser-induced damage in optical components. The kinetic properties of material ejected as a result of localized laser energy deposition are still not sufficiently resolved. Such information could enable more accurate predictions of the quantity of material removed and the spatiotemporal distribution of material re-deposition. Specifically, in laser ablation, the ejected particles resulting from a first pulse can interfere with the subsequent pulse leading to a decline in the predicted ablation speed.[1-3] In thin film laser deposition, larger particles formed from the ablation process accumulate on the film deposition area causing degradation of film quality.[4-7] In the case of laser-induced damage, the ejected particles can become a source of contamination for or even mechanical damage of adjacent optical components. This is particularly important in large aperture laser systems where the optical components would remain in operation even after sustaining damage from the laser pulses.[8]

It has been proposed that such particles can be intercepted by another laser beam, but the development of such technology requires a precise understanding of the kinetics of the ejected material clusters.[9-10] One current hypothesis is that ejection occurs abruptly as part of an explosive boiling process.[11-13] The speed of ejecta formed during thin film deposition was previously measured using spinning wheel and pump-probe approaches, where it was assumed that all particles were ejected immediately upon arrival of the laser pulse.[14-16] A more accurate estimate of the kinetic properties of the ejected particles can be made by tracking individual particles at multiple delay times along their trajectory. This approach is implemented in this work with the aid of a time-resolved shadowgraphic microscopy system capable of acquiring images at multiple points in time during a single laser energy deposition event. We employ this system to study the kinetics of the ejected material clusters following laser-induced breakdown on the surface of fused silica, a material widely used in thin film deposition and for the manufacturing of optical components for large aperture laser systems. The results suggest that the material ejection process continues for about 10 μs from the arrival of the laser pulse and gives rise to material clusters characterized by a spectrum of sizes (1 to 30 μm) and speeds (3 to 0.001 km/s).

The output of a laser (Quanta-Ray, Spectra-Physics) operating at 355 nm (3ω), 7.5-ns full-width at half maximum (FWHM) in duration (henceforth referred to as *pump* laser), was focused about 2 cm behind the exit-surface of a 5-cm round, 1-cm thick fused silica window using a 15-cm focal length lens. The fluence at the input-surface of the sample was below breakdown threshold but, due to beam convergence, the exposure on the exit-surface was just above the breakdown threshold (~40 J/cm^2) covering an estimated diameter of ~1 mm. This procedure led to the formation of single or multiple pit craters on the order of 10-50 μm in diameter. The laser fluence at the exit-surface was kept at just above the breakdown threshold to minimize the amount of ejected material for more accurate imaging of individual particles. Time-resolved images were acquired using dual strobe-light illumination provided by two spatially overlapped 532 nm (2ω) pulses with orthogonal linear polarization states from separate lasers (Litron Lasers), ~4.5 ns (FWHM) in duration (henceforth referred to as *probe* pulses). The timing of the probe pulses with respect to that of the pump pulse was controlled via adjustable external triggers. With this arrangement, we defined τ_1 as the time delay of the first probe pulse relative to the peak of the pump pulse and $\Delta\tau$ as the relative time delay between the two probe pulses. While the shot-to-shot timing jitter between pump and probe pulses was ~2 ns, the above delays were precisely recorded for each damage event with ~0.5 ns resolution. The images were acquired using a microscope system comprised of a long working distance 5X objective (Mitutoyo) followed by a 5X zoom lens. The focal plane of a microscope was set perpendicular to the sample's exit surface and adjusted to coincide with the location of the ejected material clusters. The image formed by the microscope's optics was subsequently split using a polarizing beam-splitter to separate the two orthogonal polarization image components, each arising from the separate probe pulses, and captured using charge-coupled devices (CCD, Spiricon, 1616 pixels × 1216 pixels) with individual pixel size of 4.4 μm. The resulting images covered a 755 μm × 569 μm field of view with static optimal resolution better than 2 μm and with a depth of

focus of ~40 µm. Further details on the design of this microscope system can be found elsewhere.[17]

Figure 1 shows a typical image during a surface breakdown event recorded at 100 ns delay using the illumination of probe 1. At this delay, particles with diameters less than 5 µm were observed to be well separated from the surface. The "fastest" particles, observed on the right hand side of the image, are ~1-2 µm in diameter and are traveling with a speed on the order of ~2 km/s. Also visible at this early delay time is the shock-front which is observed to be traveling ahead of most particles. Due to the time duration (~4.5 ns) of the probe pulse, the fastest particles are perceived as elongated features along their paths (observed length = speed × exposure time ≈ 9 µm).

Figure 2(a) shows an image at 2.0 µs delay using the illumination of probe 1. The particles appear to form a well-defined jet at later delay times (> ~75 ns). Figure 2(b) shows the image of the same event recorded at 2.5 µs delay using the illumination of probe 2. The relative positions of the particles do not significantly change between these two delay times, allowing for identification and tracking of most particles from the first image to the second; for easier visualization of this result, circles (red) and squares (blue) in Figs. 2(a-b) were added to indicate the same groups of particles. This tracking ability also reveals the 3-dimensional structure and motion of the particles, as seen in the magnified images shown in the inset of each image. Namely, some particles exhibit a high aspect ratio, i.e., they resemble flakes or irregularly-shaped particles rather than quasi-spherical particles, and they rotate during their propagation.

The average speed of a particle $\mathbf{v}_{avg}$ can be computed based on individual images as the distance traveled from the sample's surface divided by the time delay of the corresponding probe, i.e., similar to the speeds via other methods such as those discussed in the introduction. A more accurate estimate of the particle's instantaneous speed is given by $\mathbf{v}_{est} = (s_2-s_1)/\Delta\tau$, where (s_2-s_1) is the relative distance traveled by the particle from the surface during the time interval between the probe pulses ($\Delta\tau$).

Figure 3 shows the distribution of estimated particle speeds, $\mathbf{v}_{est}$, and sizes at various time delays τ_1 (corresponding to the image in which the particle was first observed). Particles up to 3 km/s and with diameters less than 5 µm are observed in the images at earlier delay times (as also shown in Fig. 1). At later delays, particles with diameter up to ~30 µm can be observed. Particle speed decreases to ~100 m/s by around 500 ns delay and continues to decrease to ~10 m/s for images recorded at delays on the order of 10 µs. A jet of ejected particles was observed for delays up to ~10 µs for breakdown events on a pristine surface and ≥ ~20 µs or longer for breakdown events on pre-damaged surface sites (also referred to as damage growth).

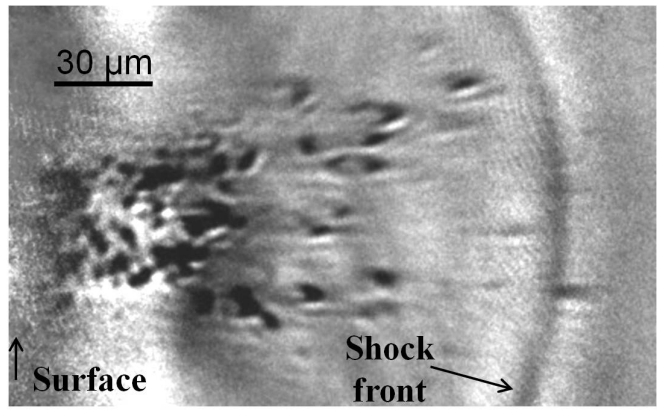

FIG. 1. Typical image captured at a delay time of 100 ns following a surface breakdown event.

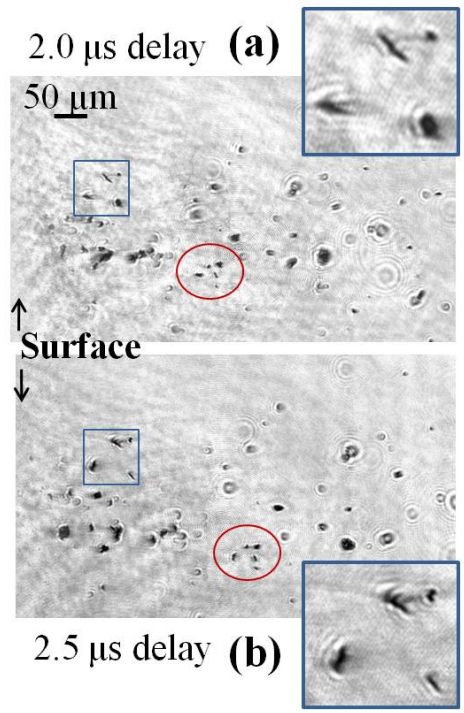

FIG. 2 (Color online.) Typical images of ejected particles from a surface breakdown event at (a) 2.0 µs delay and (b) 2.5 µs delay. Circles and squares in both images aid in visual tracking of the same two groups of particles, respectively.

The accuracy of $\mathbf{v}_{avg}$ depends on two assumptions, namely that the particle i) is ejected at t=0 (arrival of the pump pulse and ii) travels at constant speed after ejection. By plotting the ratio $\mathbf{v}_{avg}/\mathbf{v}_{est}$ the deviation of this ratio from unity can be examined. Figure 4 illustrates the average value of $\mathbf{v}_{avg}/\mathbf{v}_{est}$ as a function of the delay time. Each data point represents the mean value of the ratio for all particles confined within 200 µm from the surface, as observed in the images recorded at each delay time. For early delays (up to ~500 ns), the particles observed in the images exhibit a

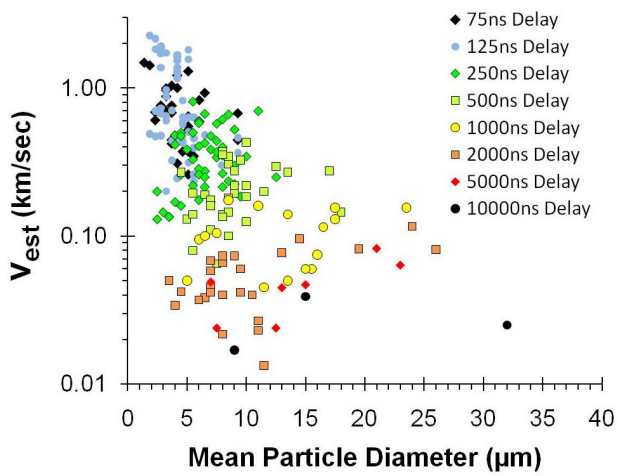

FIG. 3. (Color online.) Distribution of estimated particle speeds and sizes at various delay times.

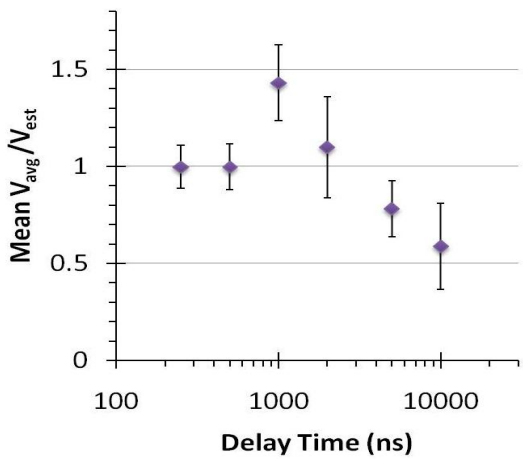

FIG. 4. Plot of ratio of average speed $\mathbf{v}_{avg}$ to estimated speed $\mathbf{v}_{est}$ versus delay time. Error bars indicate one standard deviation from the mean value within the specified delay time group.

speed ratio value close to 1, thus indicating i) a low loss of kinetic energy and ii) the ejection time was close to zero delay. At 1 µs delay, the particles exhibit a ratio significantly larger than 1. This indicates that the instantaneous speed (estimated by $\mathbf{v}_{est}$) is lower than $\mathbf{v}_{avg}$ suggesting a strong deceleration effects for this group of particles. As illustrated in the image shown in Fig. 2, there are larger particles observed at delays longer than about 1 µs. As our experiment was performed in air, the presence of deceleration by these larger and irregularly-shaped particles while traveling through the air is not surprising. However, at later delays (>5 µs), this deceleration effect seems to be countered by a different process as the ratio decreases well below 1. This opposing effect is probably not due to 'delayed' particle acceleration, since the shock front at these late times has long since traversed the field of view. We postulate instead that this effect arises from a delayed ejection time of the observed particles, i.e., not at t=0. As a result, the actual speed (best approximated by $\mathbf{v}_{est}$) is higher than $\mathbf{v}_{avg}$ leading to a speed ratio below 1. Assuming $\mathbf{v}_{est}$ as the actual speed of these particles and using their as-measured distance traveled, we can obtain an approximate duration of the particle ejection process. We estimate that for breakdown events on a pristine surface for the fluences used in this experiment, the ejection process continues for about 4 µs, while for breakdown events on pre-damaged surface sites at similar or lower laser fluences, it continues for about 20 µs or longer.

The kinetic properties of the ejected particles need to be considered for various applications such as thin film deposition and laser-induced damage. Of importance are also the physical properties of the ejecta including their temperature (relating to the evaporation rate during propagation in air or vacuum), their mechanical properties (relating to attachment and possibly mechanical damage upon impact on a substrate or adjacent optical element), and their optical properties (relating to how they might interact with subsequent laser pulses).

This work was performed under the auspices of the U.S. Department of Energy by
Lawrence Livermore National Laboratory under contract DE-AC52-07NA27344.

[1] J. Konig, S. Nolte, and A. Tunnermann, Opt Express **13,** 10597-10607 (2005).
[2] G. Raciukaitis, M. Brikas, P. Gecys, and M. Gedvilas, Proc SPIE **70052L** (2008).
[3] A. Ancona, S. Doring, C. Jauregui, F. Roser, J. Limpert, S. Nolte, and A. Tunnermann, Opt Lett **34,** 3304-3306 (2009).
[4] W. P. Barr, J Phys E **2**, 1112 (1969).
[5] M. D. Strikovsky, E. B. Klyuenkov, S. V. Gaponov, J. Schubert, and C. A. Copetti, Appl Phys Lett **63,** 1146-1148 (1993).
[6] D. B. Chrisey and, G. K. Hubler, *Pulsed Laser Deposition of Thin Films* (Wiley, New York, 1994).
[7] S. Heiroth, J. Koch, T. Lippert, A. Wokaum, D. Gunther, F. Garrelie, and M. Guillermin, J Appl Phys **107,** 014908 (2010).
[8] A. Condor, T. Alger, S. Azevedo, et al., Proc SPIE **6720,** 672010 (2007).
[9] G. Koren, R. J. Baseman, A. Gupta, M. I. Lutwyche, and R. B. Laibowitz, Appl Phys Lett **56,** 2144 (1990).
[10] E. Gyorgy, I. N. Mihailescu, M. Kompitsas, and A. Giannoudakos, Appl Surf Sci **195,** 270-276 (2002).
[11] K. Sokolowski-Tinten, J. Bialkowskim, A. Cavalleri, and D. von der Linde, Phys Rev Lett **81,** 224-227 (1998).
[12] J. H. Yoo, S. H. Jeong, X. L. Mao, R. Greif, and R. E. Russo, Appl Phys Lett **76,** 783-785 (2000).
[13] P. Lorazo, L. J. Lewis, and M. Meunier, Phys Rev Lett **91,** 225502 (2003).
[14] H. Dupendant, J. P. Gavigan, D. Givord, A. Lienard, J. P. Rebouillat, and Y. Souche, Appl Surf Sci **43,** 369-376 (1989).
[15] K. Kuba and T. Sugihara, Appl Surf Sci **96-98,** 659-662 (1996).
[16] K. Oguri, Y. Okano, T. Nishikawa, and H. Nakano, Phys Rev B **79,** 144106 (2009).
[17] R. N. Raman, R. A. Negres, and S. G. Demos, Proc SPIE **7504,** 750418 (2009).